Appl. Phys. A (2016) 122:165
DOI 10.1007/s00339-016-9700-z

Applied Physics A
Materials Science & Processing

Facile formation of superhydrophobic aluminum alloy surface and corrosion-resistant behavior

Libang Feng[1] · Zhongna Yan[1] · Xiaohu Qiang[1] · Yanhua Liu[1] · Yanping Wang[1]

Received: 20 November 2015 / Accepted: 4 February 2016 / Published online: 22 February 2016

Abstract Superhydrophobic surface with excellent corrosion resistance was prepared on aluminum alloy via boiling water treatment and surface modification with stearic acid. Results suggested that the micro- and nanoscale hierarchical structure along with the hydrophobic chemical composition surface confers the aluminum alloy surface with good superhydrophobicity, and the water contact angle and the water sliding angle can reach 156.6° and 3°, respectively. The corrosion resistance of the superhydrophobic aluminum alloy was first characterized by potentiodynamic polarization, and then the long-term corrosion resistance was investigated by immersing the sample in NaCl solution for 90 days. The surface wettability, morphology, and composition before and after immersion were examined, and results showed that the superhydrophobic aluminum alloy surface possessed good corrosion resistance under the experimental conditions, which is favorable for its practical application as an engineering material in seawater corrosion conditions. Finally, the mechanism of the superhydrophobicity and excellent corrosion resistance is deduced.

1 Introduction

Aluminum (Al) is the most plentiful metal element in the crust, which is also one of the largest used and produced metals in the non-ferrous metal territory [1]. Because of the low density, higher specific strength, good electrical and thermal conductivity, and other excellent properties, aluminum and its alloys have been widely used in industry and our daily life, especially in aerospace and civil industries [2, 3]. However, aluminum is a very reactive metal and readily corroded in some wet and salty environments [4–6], which prevents the large-scale application of aluminum and its alloys in the wet and salty environments [7, 8]. To improve the corrosion resistance, it is desirable to form superhydrophobic coatings on the surface of aluminum and its alloys, which have been proven effective in improving the corrosion resistance of aluminum and its alloys [9–11].

A superhydrophobic surface with a water contact angle (CA) larger than 150° and a sliding angle (SA) smaller than 10° has attracted a great deal of interest in both fundamental research and practical applications due to its outstanding water-repellent property [12, 13]. Such a unique characteristic has shown wide potential applications, such as anti-corrosion [9, 14], self-cleaning, anti-bioadhesion [10, 15], anti-icing [1, 16], and oil–water separation [17]. The key factor to fabricate a superhydrophobic surface is the synergistic effect of both low-energy layer and rough hierarchical structure [18]. Up to now, various approaches have been successfully developed for fabricating of superhydrophobic surfaces, such as sol–gel process [9, 19], electrochemical anodization [20], chemical etching [21], solution immersion [22, 23], and laser fabrication [24]. For example, Zheng et al. [3] fabricated a self-cleaning superhydrophobic surface via electrochemical anodization followed by surface modification using myristic acid. Vorobyev and Guo [25] created a multifunctional metal surface by constructing a hierarchical nano-/microstructure with femtosecond laser pulses. Li et al. [26] developed a superhydrophobic aluminum alloy surface with excellent corrosion inhibition by hydrochloric acid etching, potassium permanganate passivation, and fluoroalkylsilane

✉ Libang Feng
lepond@hotmail.com

[1] School of Mechatronic Engineering, Lanzhou Jiaotong University, Lanzhou 730070, China

modification method. However, most of the techniques reported above require special equipment, complex process, or harsh chemical treatment, which seriously impede the practical application process of the fabrication methods. Thus, a simple, inexpensive, and environment-friendly preparation method is quite needed to further greatly advance the application process of the superhydrophobic aluminum alloys.

In this paper, we demonstrate a facile and environment-friendly technique for the fabrication of superhydrophobic aluminum alloy surfaces, i.e., the boiling water treatment and STA modification in DMF–H_2O solution. The whole procedure is simple to carry out, and no special equipment is required. Moreover, the method is also low cost and inexpensive, while the as-prepared superhydrophobic aluminum alloy surface possesses excellent corrosion resistance.

2 Experimental section

2.1 Materials

Commercially available 6063 aluminum alloy plates (Si: 0.20–0.60 wt%, Fe: 0.35 wt%, Cu: 0.10 wt%, M_n: 0.10 wt%, Mg: 0.45–0.90 wt%, Cr: 0.10 wt%, Zn: 0.10 wt%, Ti: 0.10 wt%, other impurities: 0.15 wt%, and the remaining is Al) with a size of 20 mm × 10 mm × 2 mm were used as the substrates. Stearic acid (STA) was obtained from Sinopharm Group Chemical Reagent Co., Ltd. *N*,*N*-dimethylformamide (DMF) was obtained from Shanghai Chemical Reagent Co., Ltd. Acetone and methanol were obtained from Tianjin Benchmark Chemical Reagent Co., Ltd. (China).

2.2 Fabrication of the superhydrophobic aluminum alloy surfaces

The superhydrophobic Al alloy surfaces were fabricated by a facile and environment-friendly method, and the schematic illustration is shown in Scheme 1. Prior to modifying with STA, aluminum alloy plates were polished mechanically using $800^{\#}$, $1000^{\#}$, and $1500^{\#}$ metallographic abrasive paper in turn to remove the oxide/hydroxide layer and impurities at the surfaces and then sequentially cleaned using methanol, acetone, and deionized water for about 10 min under ultrasonication, respectively. After dried, surfaces of the aluminum alloy plates were allowed to roughen using the boiling water for 5 min. Finally, the aluminum alloy plates were immersed in 1:1 volume mixture of DMF–H_2O solution containing 10 mmol/L of STA at the temperature of 65 °C. Afterward, the resulting plates were rinsed with DMF and deionized water and then dried in air at room temperature for several hours prior to further characterization. Thus, the superhydrophobic aluminum alloys were fabricated.

2.3 Sample characterization

The water contact angles (CAs) and sliding angles (SAs) of the as-prepared surfaces were measured using a horizontal microscope with a protractor eyepiece (DSA 100, Kruss, Germany) at room temperature, while a water droplet with a volume of 8 μL was applied to the measurements. The contact angle was adopted as the average value for one sample at five fresh positions. The sliding angle was measured and recorded by tilting the stage when the droplet began to roll in the downhill direction.

Morphology of the as-prepared Al alloy surface was observed by a field emission type of scanning electron microscope (FE-SEM, JSM-6701F, Japan), and the element composition was characterized by energy-dispersive spectrometer (EDS) associated with the FE-SEM instrument.

The phase and chemical composition of the sample were investigated by characterizing the powder scraped from Al alloy surface with X-ray diffractometry (XRD-7000, Shimadzu, Japan) and Fourier transform infrared spectroscopy (FTIR, VER-TEX 70, Bruker, Germany), respectively.

Both the immersion experiments and electrochemical measurements were taken to examine the corrosion-resistant performance of the resulted Al alloys. The electrochemical measurements were taken in 3.5 wt% of NaCl solution using a computer-controlled electrochemical workstation (CHI660D, CH Instruments Inc.) at room temperature in a traditional three-electrode cell. The as-prepared surface with a size of 1 cm × 1 cm was used as the working electrode, while a platinum plate and saturated calomel electrode were used as counter electrode and reference electrode, respectively. The polarization curves were established at a sweep rate of 10 mV/s, and the corrosion potential (E_{corr}) and corrosion current density (I_{corr}) were obtained using the Tafel extrapolation method.

3 Results and discussion

3.1 Analysis of the fabrication and superhydrophobicity

The superhydrophobic aluminum alloy surface was fabricated using a facile and environment-friendly technique, i.e., the boiling water treatment and STA modification in DMF–H_2O solution. No caustic reagents and special equipment are used in the whole preparing procedure. Therefore, the fabrication work is quite easy to put into practice. The preparation steps have distinct influence on

Scheme 1 Schematic illustration for fabricating the superhydrophobic Al alloy surface

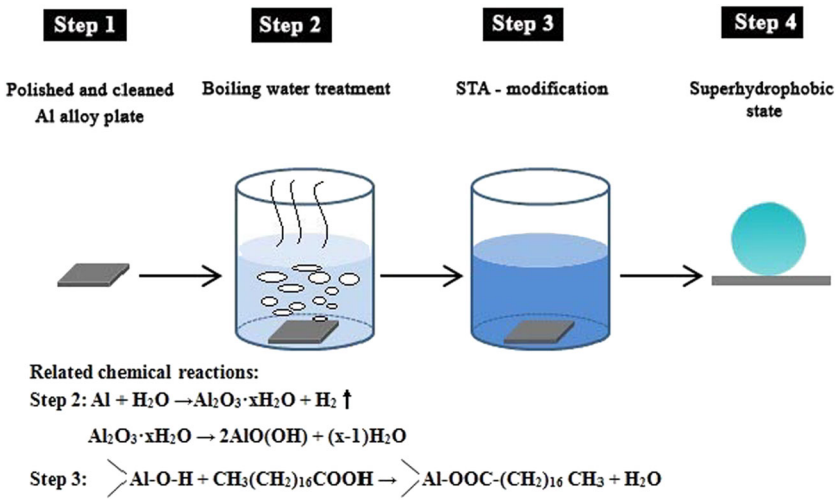

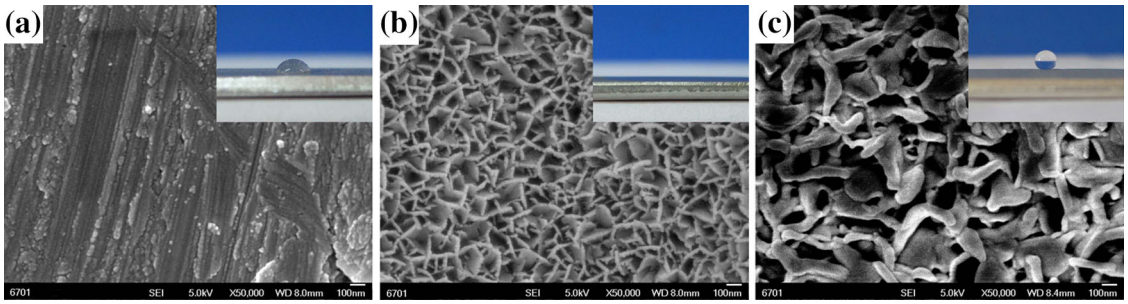

Fig. 1 SEM micrographs of the aluminum alloy surfaces after different treatment steps, while inserts are the wetting images: **a** untreated, **b** boiling water treatment, and **c** STA modification

the microstructure, wettability, and chemical structure at the aluminum alloy surfaces, which have been investigated using SEM, contact angle measurement, and FTIR techniques, respectively.

The SEM micrographs of the aluminum alloy surfaces after different treatment steps are shown in Fig. 1. It can be found from Fig. 1a that the micrograph of the untreated aluminum alloy surface shows a relatively smooth structure. However, the microstructure of the aluminum alloy surface changes greatly after the boiling water treatment, and a quiet rough structure with a great quantity of pores presents (see Fig. 1b). After the aluminum alloy plate is immersed in the boiling water, some chemical reactions happen, just as the related reaction equations shown in Scheme 1. Thus, the reason that leads to the result can be deduced as follows: the Al begins to reacts with the boiling water immediately once the aluminum alloy plate is immersed in the boiling water. Thereupon, $Al_2O_3 \cdot xH_2O$ and H_2 generate. The generated H_2 can break through some loose $Al_2O_3 \cdot xH_2O$, while some $Al_2O_3 \cdot xH_2O$ can further react with the boiling water to form boehmite (AlO(OH)), which is easy to dissolve in the boiling water. Thereafter, the rough and porous structure is fabricated [8, 23]. Figure 1c shows the morphology of the as-prepared aluminum alloy surface after immersed in 1:1 volume mixture of DMF–H_2O solution containing 10 mmol/L of STA at 65 °C. It can be found that the surface becomes much coarser as compared to that of the aluminum alloy surface treated with the boiling water, and many hierarchical rough structures that consist of wormlike ridges and pores form upon the porous and rough aluminum alloy plates.

Additionally, the water contact angle (CA) at the aluminum alloy plates after different treatment steps is investigated and the corresponding images are inserted in SEM images in Fig. 1, which clearly demonstrates the change of the wettability at the aluminum alloy surfaces upon different treatment steps. The CA at the untreated aluminum alloy surface is ca. 78.2°, while the water droplet completely spreads on the aluminum alloy plates (namely, the CA is approximately 0°) after treated in the boiling water, indicating the aluminum alloy plate surface takes on superhydrophilicity at this moment. However, the wettability at the aluminum alloy surface changes remarkably after STA modification. The water droplet settles on the surface with perfect sphere-like shape, and the CA and sliding angle (SA) reach 156.6° and 3°, respectively. These

manifest that the resultant aluminum alloy surface takes on the superhydrophobicity.

Therefore, it can be found that the boiling water treatment endows the aluminum alloy surface with the rough and porous structure, while STA modification endues the aluminum alloy surface with the hierarchical rough structure grafted with the low surface energy materials (the related reaction equation is shown in Scheme 1). So the results indicate that both the boiling water treatment and STA modification are important in the formation of the superhydrophobic aluminum alloy surfaces.

The cleaned Al alloy is a hydrophilic material with a CA of 78.2°. After obtaining the rough and porous structure upon the boiling water treatment, the aluminum alloy surface exhibits superhydrophilic property. This result clarifies the assumption proposed by Wenzel that rough surface structure can enhance the hydrophilicity of a hydrophilic surface [27].

According to Wenzel's equation [28]:

$$\cos\theta_r = r \cdot \cos\theta \quad (1)$$

where θ_r and θ are the contact angles of liquid droplets on the rough and smooth solid surfaces made of the same materials, respectively, while r is the roughness factor defined as the ratio between the real and projected solid–liquid contact areas, and r is always larger than 1. Since there are large numbers of pores produced by the boiling water treatment, the surface roughness of the aluminum alloy has greatly increased. Meanwhile, $Al_2O_3{\cdot}xH_2O$ and boehmite both exhibit hydrophilic. Therefore, the aluminum alloy surface takes on superhydrophilicity.

On the other hand, the surface chemical structure also has much influence on the surface wettability. So the Fourier transform infrared spectroscopy (FTIR) was utilized to investigate the chemical composition on the aluminum alloy surfaces. Figure 2 shows the FTIR spectra of the untreated aluminum alloy, as-prepared aluminum alloy, and stearic acid. As compared to the untreated aluminum alloy surfaces (see Fig. 2a), several quite distinct absorption peaks present at the IR spectrum of the as-prepared aluminum alloy surface (as shown in Fig. 2b). Thereinto, two absorption peaks at 2920 and 2851 cm^{-1} are ascribed to the symmetric and asymmetric stretching vibration of $–CH_2–$ groups in STA, respectively, as these two peaks just appear in the IR spectrum of STA (see Fig. 2c). Additionally, two new peaks present at 1470 and 1380 cm^{-1}, which are attributed to the absorption of $–CH_2–$ and $–CH_3$ groups, respectively. More importantly, the absorption peak of free $–COO^-$ groups in STA molecule presents at 1700 cm^{-1} (see Fig. 2c). By contrast, this peak moves to 1585 cm^{-1} in the IR spectrum of the as-prepared aluminum alloy surface (as shown in Fig. 2b). The movement of the $–COO^-$ absorption peak manifests that the reaction

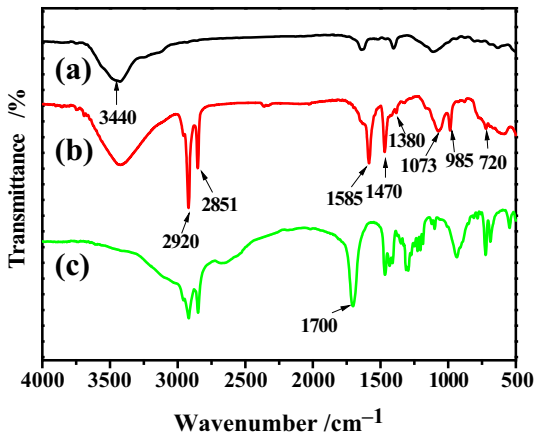

Fig. 2 FTIR spectra of the aluminum alloy and stearic acid: **a** untreated aluminum alloy, **b** as-prepared aluminum alloy, and **c** STA

between the carboxyl groups in STA and Al–OH at the aluminum alloy surface has taken place successfully. Thereupon, this peak is assigned to the absorption of –COO–Al groups. As a result, the long alkyl chains in STA are chemically grafted onto the aluminum alloy surface as expected, and it reveals the presence of $CH_3(CH_2)_{16}COO–$Al with low surface free energy at the as-prepared surface [23, 29].

As a conclusion, the superhydrophobicity of the as-prepared aluminum alloy surface mainly comes from the presence of the heterogeneous rough structure and low surface energy material at the surface. The water droplet with a size far larger than the microstructure is actually in contact with both the STA modification film and air, while it cannot penetrate into the pores among the rough structure and might be suspended on those rough structures. This state can be described by Cassie–Baxter equation [30]:

$$\cos\theta_r = f_1\cos\theta - f_2 \quad (2)$$

where θ_r and θ denote the contact angles of liquid droplets on the STA-modified rough and smooth solid surface made of the same materials, respectively, while f_1 and f_2 are the area fractions estimated for the solid and the air trapped between STA-modified aluminum alloy surface and a water droplet, respectively (i.e., $f_1 + f_2 = 1$). This equation also demonstrates that the larger the air fraction (f_2), the more hydrophobic the surface is. In our study, θ is estimated as 100.1° and θ_r is 156.6°. So f_1 and f_2 are estimated to be 0.0997 and 0.9003, respectively. These data indicate that when a water droplet is settled on the superhydrophobic aluminum alloy surface, approximately 9.97 % serves as the contact area of the water droplet and solid surface, and the remaining 90.03 % serves as the contact area of the water droplet and air [8].

3.2 Effect of the volume ratio of DMF–water on the wettability and microstructure

The boiling water treatment has too much influence on the aluminum alloy surface wettability and microstructure, which has been revealed by water contact angle measurement and SEM observation [14, 26]. Results reveal that the optimal treatment time is 5 min. Similarly, the volume ratio of DMF to water also has distinct influence on the aluminum alloy surface wettability and microstructure, and changes of the CA and morphology at the aluminum alloy surface with volume ratio of DMF to water are shown in Figs. 3 and 4, respectively.

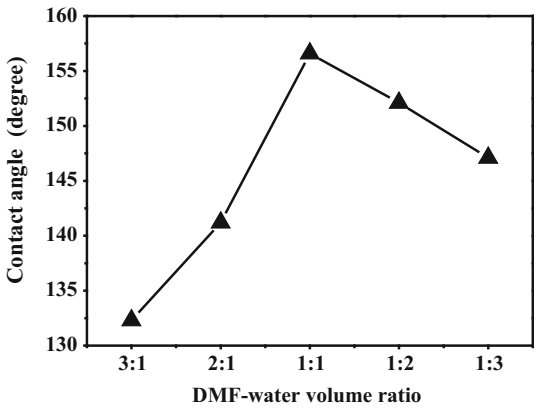

Fig. 3 Effect of DMF–water volume ratio on water contact angle

Figure 3 shows the change trend of the CA at the aluminum alloy surface upon different volume ratios of DMF–water containing 10 mmol/L of STA at 65 °C for 24 h. It can be found from Fig. 3 that the CA is only 132.3° when the volume ratio of DMF–water is 3:1, while it increases gradually with the decrease in the volume ratio of DMF to water. The CA gets 156.6° when the volume ratio of DMF–water reaches 1:1. However, the CA falls by degrees with the volume ratio decreases further. So the results indicate that the optimal ratio between DMF and water is 1:1, and the reason can be explained as follows: when the boiling water treated Al alloy is modified by STA–DMF–H_2O at 65 °C, the Al can be further oxidized because the different DMF–H_2O volume ratios have different dissolving capacities to STA and further provide different amounts of water in oxidizing Al surface. Thus, the aluminum surface is etched by various degrees and the different surface morphologies are resulted accordingly with the different DMF–water ratios. Thereupon, when the DMF–water volume ratio is 1:1, the appropriate amount of water and dissolved STA are reached. Consequently, the suitable structure at the aluminum alloy surface is obtained, and then the superhydrophobic surface is resulted.

Figure 4 shows the SEM micrographs of the aluminum alloy surface upon different volume ratios of DMF to water. It can be noted that a netlike structure with lots of pores crossed by ridges comes into being when the volume ratio of DMF to water is 3:1 as shown in Fig. 4a, which

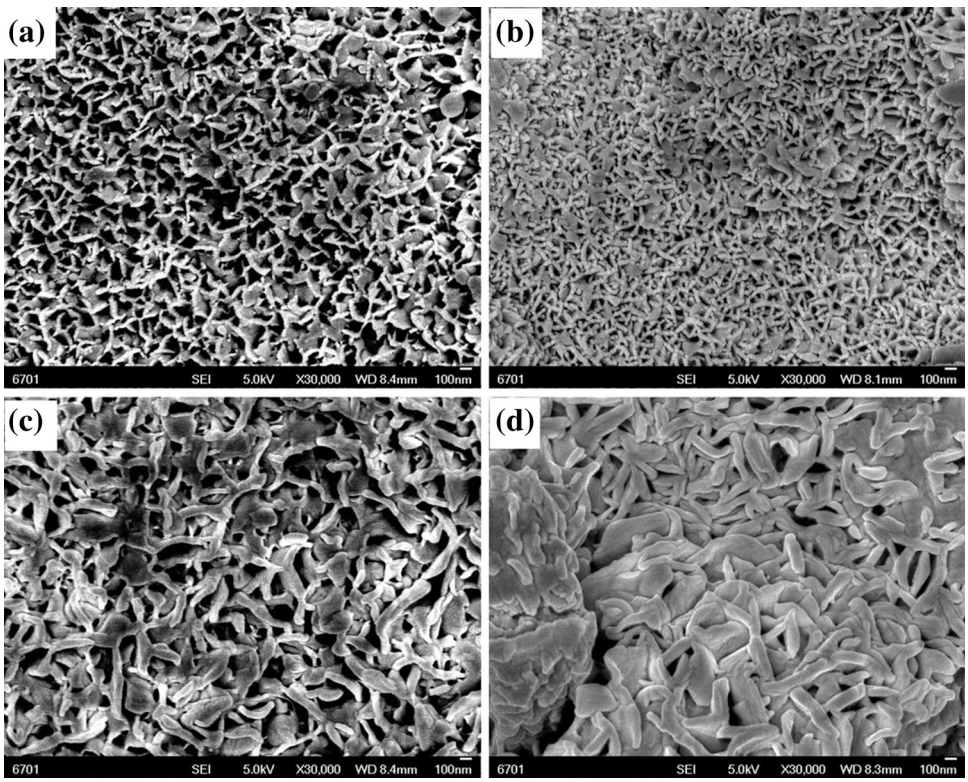

Fig. 4 SEM micrographs of the aluminum alloy surface upon different volume ratios of DMF to water: **a** 3:1, **b** 2:1, **c** 1:1, and **d** 1:2

almost has no marked difference with the aluminum alloy surface only treated by the boiling water for 5 min (without grafting STA, see Fig. 1b), which indicates that the STA chains may not successfully grafted onto the aluminum alloy surface at this volume ratio. Accordingly, the aluminum alloy surface cannot achieve the superhydrophobicity. The morphology begins to exhibit the distinct difference when the volume ratio of DMF to water increases to 2:1, as shown in Fig. 4b. It can be found that the porous and rough morphology with nano-rods and lamellar structure presents. When the volume ratio of DMF to water increases to 1:1, it can be found from Fig. 4c that many fluctuant and protuberant ridges link together, which forms the hierarchical rough structure with many micro- and nano-pores. As a result, the as-prepared aluminum alloy surface possesses the superhydrophobicity with a CA of 156.6°. However, with the volume ratio of DMF to water continues to decrease to 1:2, the morphology of the uneven and imporous structure engenders at the aluminum alloy surface due to the nano-rods and lamellar structure assembling disorderly. Hence, the micro- and nano-pores scarcely appear, as shown in Fig. 4d. The reason that leads to this result might be when the volume ratio of DMF to water decreases, the amount of water increases, while the amount of the solved STA in the mixed solution decreases. Whereafter, the water excessively reacts with the treated rough aluminum alloy surface, but there is not enough STA to modify and graft on the rough structure. Therefore, the flowerlike structure cannot be formed under this condition and the superhydrophobicity cannot be achieved at the surface.

3.3 Effect of STA modification time on the wettability and microstructure

The STA modification time also has remarkable influence on the aluminum alloy surface wettability and microstructure. To explore the effect of the STA modification time on the wettability and microstructure, the clean aluminum alloy plates treated with the boiling water were chemically modified in the 1:1 volume ratio of DMF to water containing 10 mmol/L of STA at 65 °C for 1, 5, 10, 15, 24, 36, and 48 h. The obtained results are shown in Figs. 5 and 6, respectively.

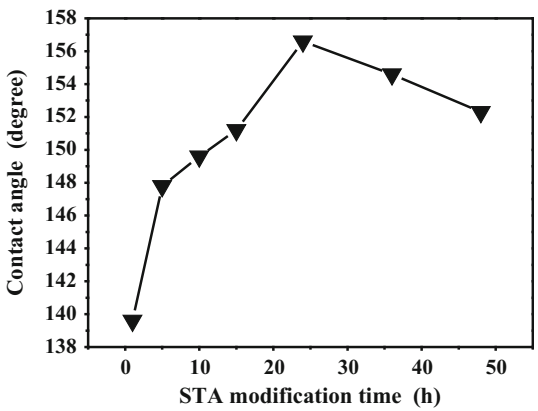

Fig. 5 Water contact angle upon the STA modification time

Figure 5 shows the variation of the CA with the STA modification time. It reveals that the CA significantly enhances from 139.6° to 156.6° when the STA modification time increases from 1 to 24 h. By contrast, the CA does not further increase any longer and conversely begins to decrease when the STA modification time continues to extend, and the CA decreases to 152.3° while lengthening the modification time to 48 h. Therefore, the optimal STA modification time is 24 h and the superhydrophobic aluminum alloy surface with a CA of 156.6° is resulted.

Figure 6 shows SEM micrographs of the aluminum alloy surface with the different STA modification time. Nano-rods and lamellar structure link together, and there is hardly any micro- and nano-pores at the surface for 5 h of STA modification, as shown in Fig. 6a. The flowerlike structure with large amount of ridges and pores appears at the surface when further increasing the STA modification time to 15 h (see Fig. 6b), and the space between the lamellar is 60–300 nm, while the lamellar thickness is 20–60 nm. Meanwhile, it can be seen from Fig. 6c that many fluctuant and protuberant ridges linked together form the uniformly flowerlike structure with many micro- and nano-pores, which contributes to the highest CA of 156.6° upon the STA modification of 24 h. Figure 6d shows that the significantly change and the prominent ridges of the flowerlike structure have grown bigger and thicker when the STA modification time reaches 48 h, where the space between lamellar and the thickness of lamellar itself is 20–200 and 40–300 nm, respectively. This greatly reduces the amount of micro- and nano-pores or the roughness of the aluminum alloy surface. Thereupon, the water repellence is poorer than that of the 24-h modification. Such phenomenon can be explained in terms of Cassie–Baxter equation [see Eq. (2)]. Given that θ is 100.1°, θ_r is 147.8°, 151.2°, 156.6°, and 152.3° for the STA modification time of 5, 15, 24, and 48 h in turn. Accordingly, the air fraction of f_2 is estimated to be 0.8135, 0.8499, 0.9003, and 0.8610, respectively, which indicates that the change of CA corresponds to the amount of air trapped at the composite interface. These results show that the maximum amount of air has been trapped within the flowerlike rough surface with 24 h of STA modification as compared to the others. Thereupon, the heterogeneous surface with 24 h of STA modification possesses the excellent water-repellent behavior.

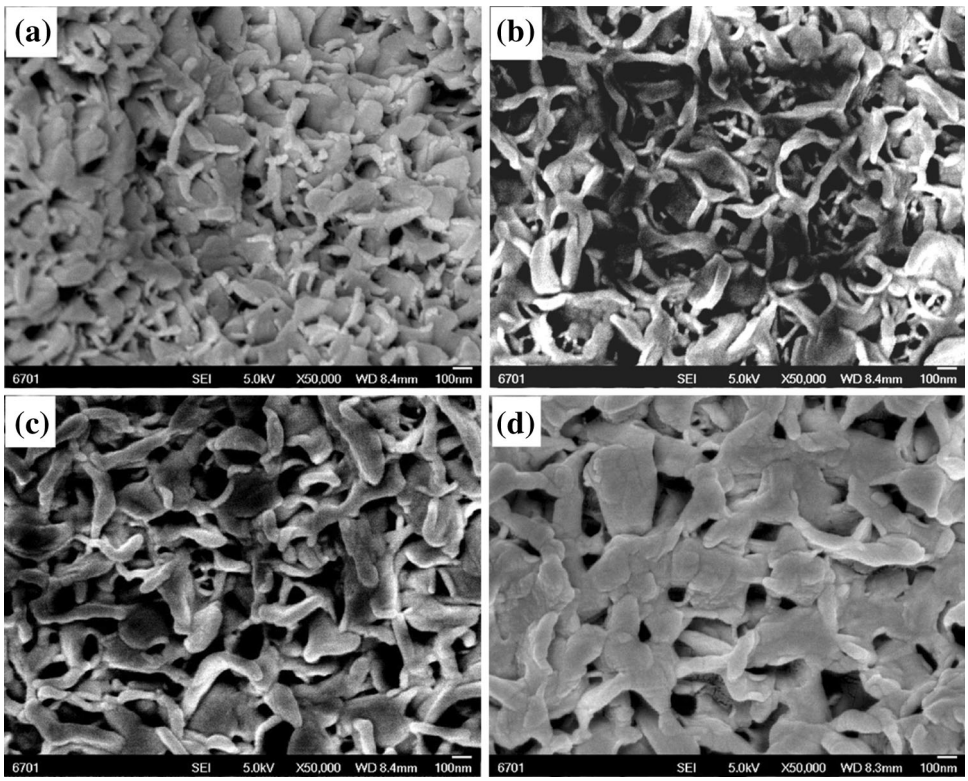

Fig. 6 FE-SEM micrographs of the aluminum alloy surface with different STA modification time in STA–DMF–H_2O solution: **a** 5 h, **b** 15 h, **c** 24 h, and **d** 48 h

3.4 Microstructure and the water repellence of the superhydrophobic aluminum alloy surface

Figure 7 shows SEM images with different magnifications of the as-prepared aluminum alloy surface with the superhydrophobicity. Meanwhile, the digital photograph of water droplets on the superhydrophobic aluminum alloy plates together with the corresponding photographs of the CA and SA of a water droplet is also shown in Fig. 7. It can be found from Fig. 7a that the surface presents quite even micrograph, while the surface is composed of a large quantity of well-distributed wormlike structure. The higher magnification micrograph (see Fig. 7b) shows that the aluminum alloy surface consists of lots of 3D flowerlike microstructure, while the flowerlike structure is linked and divided into micro- and nano-porous structure by a number of ridges. Meanwhile, the size of the pore is between 100 and 260 nm in diameter and the lamellar thickness is 40–70 nm. Thus, after STA modification, the flowerlike heterogeneous rough structure with numbers of ridges and pores forms at the aluminum alloy surface, which indicates that the resultant superhydrophobic surface takes on the micro- and nano-dual scales' structure.

Just grounded on the micro- and nano-dual scales' heterogeneous structure and the grafted long $C_{17}H_{35}COO$-alkyl chains, the resultant aluminum alloy plate exhibits excellent superhydrophobic property. Therefore, the water droplet placed on the as-prepared aluminum alloy surface presents with the perfect spherical shape (as shown in Fig. 7c). Additionally, a great quantity of air is trapped in the pores among linked and divided ridges. Consequently, the resultant aluminum alloy surface takes on strong water repellence with both high CA and low SA.

3.5 Corrosion resistance of the superhydrophobic aluminum alloy surface

In order to investigate the corrosion-resistant property of the as-prepared superhydrophobic Al alloy, both the immersion experiment and electrochemical measurement were taken at room temperature.

Figure 8 shows the potentiodynamic polarization curves of the Al alloys with different water contact angles (CA) in 3.5 wt% of NaCl solution, and the corrosion potential (E_{corr}) and corrosion current density (I_{corr}) obtained using the Tafel extrapolation method are listed in Table 1.

It can be clearly seen from Fig. 8 and Table 1 that the corrosion potential (E_{corr}) of the aluminum alloy positively increases, while the corrosion current density (I_{corr}) decreases with the increase in the CA. Generally, a higher corrosion potential or a lower corrosion current density corresponds to a lower corrosion rate and a better corrosion resistance. Therefore, the shift of the E_{corr} in the positive direction and the decrease in I_{corr} could be associated with the protective property of the water-repellent coating

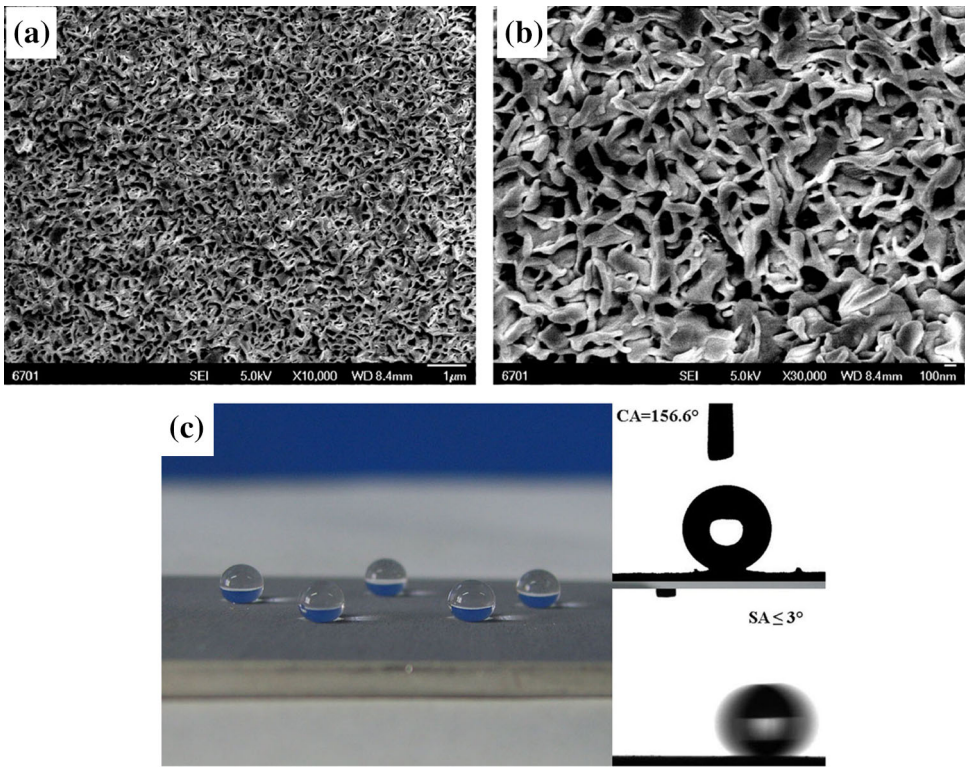

Fig. 7 **a**, **b** SEM micrographs of the superhydrophobic aluminum alloy surface with different magnifications, **c** image of water droplets on the substrate, and *insets* show the photograph of contact angle and sliding angle of a water droplet

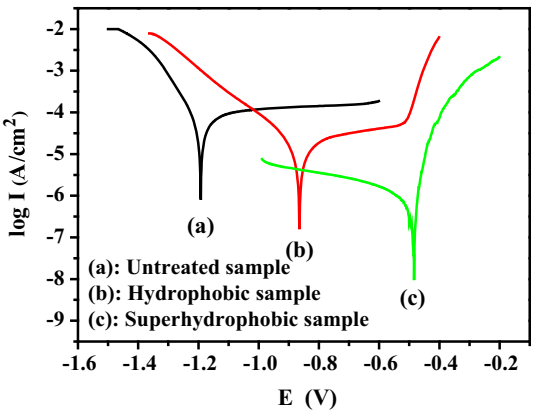

Fig. 8 Polarization curves of the aluminum alloy samples with different water contact angles: **a** 78.2°, **b** 113.3°, and **c** 156.6°

Table 1 Corrosion potential (E_{corr}) and corrosion current density (I_{corr}) of the aluminum alloy samples in 3.5 wt% NaCl solutions

Sample and its CA	E_{corr} (V)	I_{corr} (A cm^{-2})
Untreated (78.2°)	−1.18 ± 0.02	1.541×10^{-5}
Hydrophobic (113.3°)	−0.87 ± 0.02	4.227×10^{-6}
Superhydrophobic (156.6°)	−0.49 ± 0.02	2.009×10^{-7}

formed by both the micro- and nanoscale hierarchical structure and the chemically grafted hydrophobic alkyl chains, just as shown in Fig. 14, which is well related to the interfacial air cushion formed between the solid and liquid interfaces as well. When the water contact angle becomes higher, more air will be trapped between the interfaces of solid/liquid. For the aluminum alloy with the largest water contact angle, the maximum amount of air will be trapped between the solid and liquid interfaces. Therefore, the corrosive medium (such as Cl^- dissolved in water) can be hindered to penetrate into and reach the Al substrate. Thus, the lower corrosion rate is resulted. Thereupon, it can be concluded that the aluminum alloy with higher water contact angle has better corrosion resistance, and the superhydrophobic Al alloy sample (with a CA of 156.6°) exhibits the best corrosion resistance.

Additionally, the aluminum alloys are immersed in 3.5 wt% of NaCl solution for different time, and then the surface morphology, microstructure, wettability, phase structure, and chemical composition are investigated. By comparing and analyzing the difference and change of the structure and composition, the corrosion-resistant behavior of the resultant superhydrophobic aluminum alloy can be further evaluated. In our research, the samples are immersed in 3.5 wt% of NaCl aqueous solution at room temperature for 0, 2, 10, 30, 60, and 90 days, respectively. After that, the samples are rinsed with deionized water and subsequently dried at room temperature.

Digital pictures for the untreated and superhydrophobic aluminum alloy after immersed in 3.5 wt% of NaCl solution for different time are shown in Fig. 9. It can be clearly

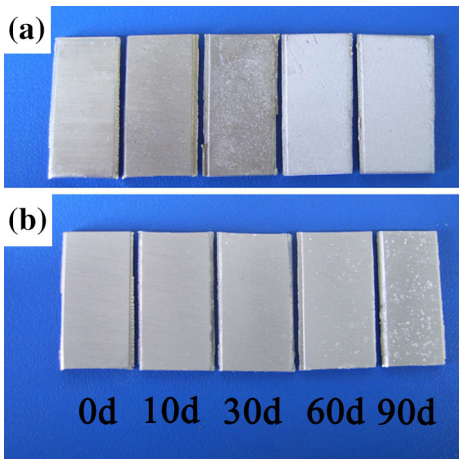

Fig. 9 Digital picture for untreated **a** and superhydrophobic **b** samples after immersed in 3.5 wt% of NaCl solution for different time

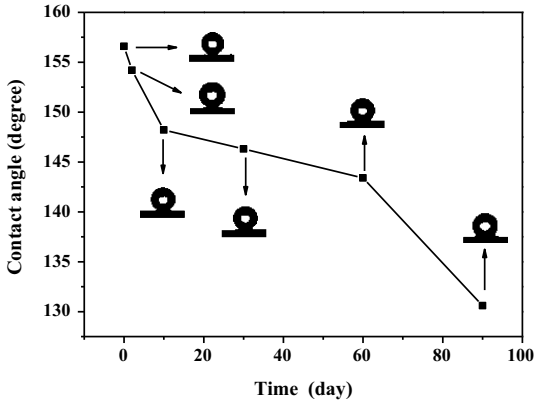

Fig. 10 Water contact angle of the superhydrophobic sample after immersed in 3.5 wt% of NaCl solution for different time

seen from Fig. 9 that as compared to the surfaces that without immersed in NaCl solution (i.e., 0 days), some so-called white corrosive products appear on the aluminum alloy surfaces. Moreover, the amount of the white corrosive products gradually increases with the immersion time extending from 0 to 90 days. More importantly, it can be found that the amount of the white corrosive products that appears on the superhydrophobic aluminum alloy surface (see Fig. 9b) is small than that on the untreated aluminum alloy surface (as shown in Fig. 9a) for the same immersion time, indicating that the corrosive degree of the untreated aluminum alloy samples is severer than that of the superhydrophobic ones.

Figure 10 exhibits the water contact angle of the superhydrophobic samples after immersed in 3.5 wt% of NaCl solution for different time. It can be found that the CA gradually decreases with the increase in the immersion time. The CA remains around 154.2° after the superhydrophobic aluminum alloy is immersed for 2 days, which indicates that the superhydrophobic aluminum alloy surface exhibits good superhydrophobicity and corrosion resistance at this corrosion condition. Furthermore, the CA at the superhydrophobic surface immersed for 90 days still remains ca. 130.6°, which just manifests that the resultant superhydrophobic aluminum alloy is hopeful for its practical application as an engineering material in seawater conditions.

In order to further explore the microstructure and chemical structure of the superhydrophobic aluminum alloy samples after immersion in 3.5 wt% of NaCl solution, the SEM and EDS techniques are used.

Typical SEM images for the untreated and superhydrophobic aluminum alloy samples before and after 90-day immersion in 3.5 wt% of NaCl solution are shown in Fig. 11. For the untreated Al alloy sample, the surface shows an quite plain structure before immersion in 3.5 wt% of NaCl solution (as shown in Fig. 11a). However, a great deal of loose new substance appears and pile up together on the surface after the sample is immersed in 3.5 wt% of NaCl solution for 90 days (Fig. 11c). For the superhydrophobic Al alloy sample, the 3D flowerlike surface with micro- and nano-pores and ridges presents before immersion in 3.5 wt% of NaCl solution (Fig. 11b). By contrast, many loose nubbly particles appear on the surface after the sample is immersed in 3.5 wt% of NaCl solution for 90 days (Fig. 11d). Meanwhile, part of 3D flowerlike structure remains all the same. However, the amount of the loose substance on the superhydrophobic aluminum alloy surfaces is less than that on the untreated ones.

Then EDS is used to estimate the chemical composition at the aluminum surface before and after immersed in 3.5 wt% of NaCl solution. Figure 12a, b shows the EDS spectra of the untreated and superhydrophobic aluminum alloy surfaces, respectively. The EDS spectrum of the untreated aluminum alloy surface in Fig. 12a shows the appearance of Al, C, O, Si, and Fe elements, while the elemental weight ratio is given in Table 2. Results indicate that the Al element holds the most part of the aluminum surface, while the elemental C might be from some methoxy groups grafted onto the aluminum alloy surface when cleaned by ultrasonication [8]. Meanwhile, it can be found from Fig. 12b and Table 2 that the Al, C, O, Si, and Fe present at the superhydrophobic aluminum alloy surface as well. As compared to the surface composition of the untreated aluminum alloy (Fig. 12a), it reveals that contents of C and O elements increase markedly, while Al content decreases remarkably, indicating that the surface composition at the aluminum alloy has taken considerable changes upon superhydrophobicity. The increase in the C and O and the decrease in the Al should result from the grafting of the STA molecules. Thereupon, it can be

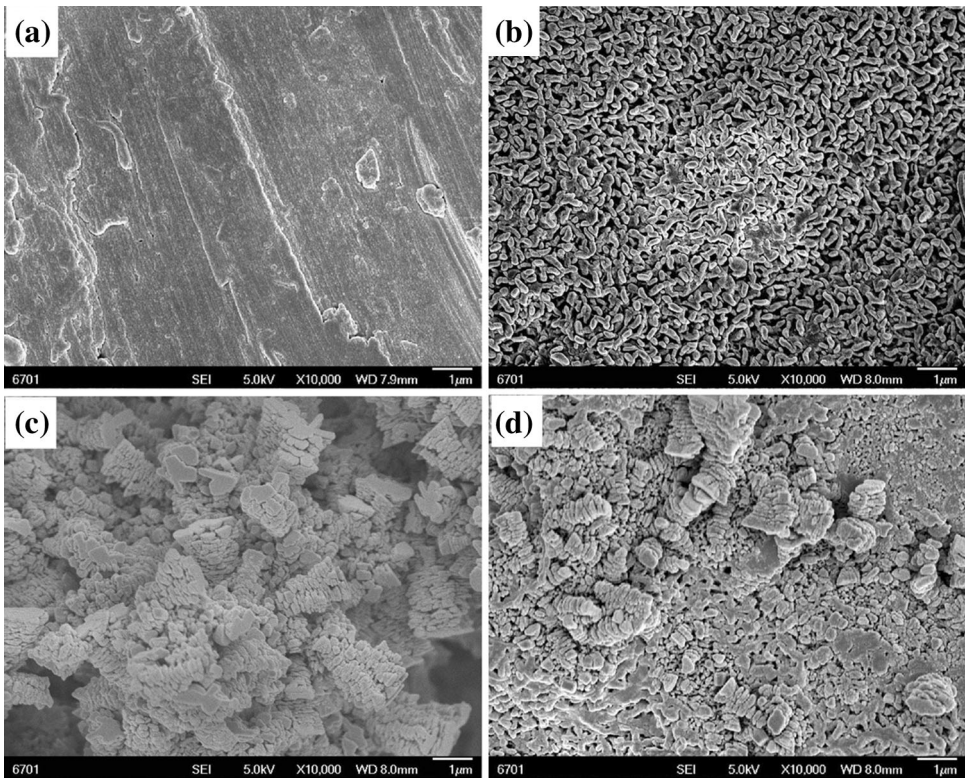

Fig. 11 SEM images for untreated (**a**, **c**) and superhydrophobic aluminum alloy samples (**b**, **d**) before (**a**, **b**) and after (**c**, **d**) 90 days immersed in 3.5 wt% of NaCl solution

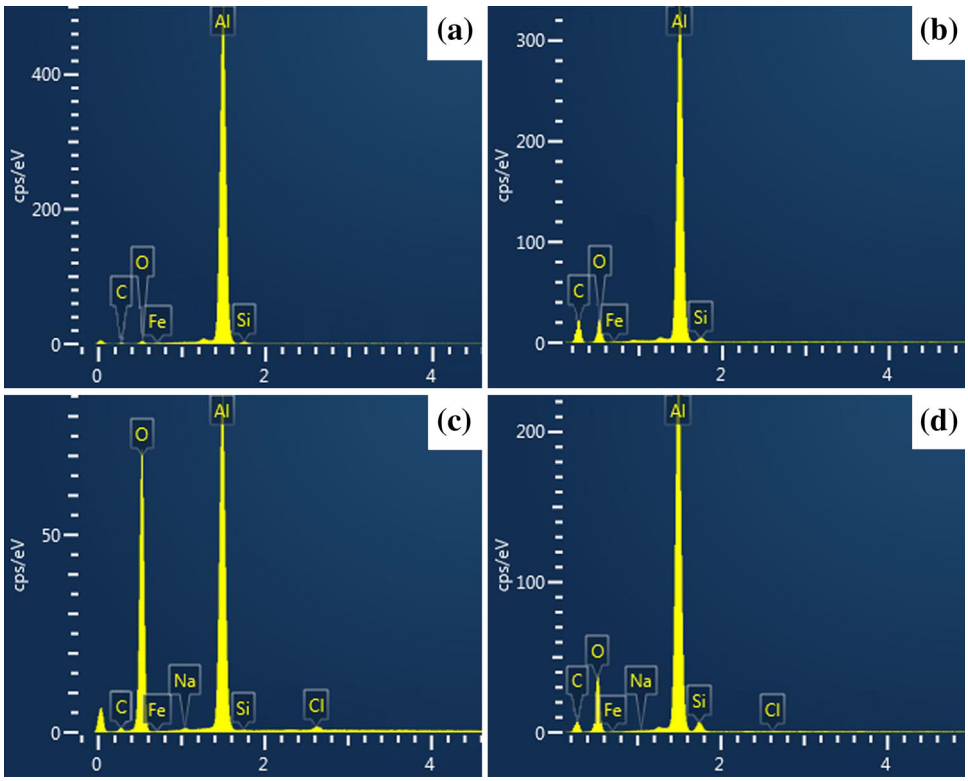

Fig. 12 EDS spectra for the untreated (**a**, **c**) and superhydrophobic aluminum alloy samples (**b**, **d**) before (**a**, **b**) and after (**c**, **d**) 90 days immersed in 3.5 wt% of NaCl solution

Table 2 The element weight ratio of the untreated and superhydrophobic aluminum alloy samples before and after 90-day immersion in 3.5 wt% of NaCl solution

Sample		Element (wt%)						
		Al	C	O	Si	Na	Cl	Fe
Untreated	0 days	83.72	10.11	4.16	1.49	0	0	0.52
	90 days	33.14	5.22	60.64	0.06	0.32	0.49	0.13
Superhydrophobic	0 days	41.25	40.69	16.77	0.81	0	0	0.48
	90 days	43.42	23.23	30.80	1.93	0.02	0.01	0.59

deduced that the long alkyl chains of STA have been anchored onto the aluminum alloy surface successfully.

Great changes take place for the aluminum alloy surface after immersion in 3.5 wt% of NaCl solution for 90 days. Figure 12c, d shows the EDS spectra for the untreated and superhydrophobic Al alloy samples after 90-day immersion in NaCl solution. As compared to the surface composition of the untreated aluminum alloy surface before immersion in NaCl solution (see Fig. 12a), the contents of Al, C, Si, and Fe elements decrease, while the content of O element increases observably for the untreated aluminum alloy surface after immersion in NaCl solution for 90 days, as shown in Fig. 12c and Table 2. Meanwhile, Cl and Na elements appear. At the same time, by comparing the surface composition of the superhydrophobic aluminum alloy before (see Fig. 12b) and after (see Fig. 12d) immersion in NaCl solution for 90 days, it can be found that the content of Al element keeps unchanged on the whole, while the content of C element decreases and the content of O element increases.

Moreover, by comparing the surface composition of both untreated and superhydrophobic Al alloy after immersion in NaCl solution (Fig. 12c, d, respectively), it can be found that there are more amount of Al and C elements and less amount of O element at the superhydrophobic aluminum alloy surface as compared to those at the untreated aluminum alloy surface. More importantly, there are a lot of amounts of Cl and Na elements at the untreated aluminum alloy surface, namely 0.49 and 0.32 wt%, respectively. By contrast, the contents of Cl and Na elements at the superhydrophobic aluminum alloy surface are only 0.01 and 0.02 wt%, respectively, indicating that very litter amount of Cl and Na elements presents.

In order to further validate the protection effect of the strong water-repellent coating and the difference in corrosion resistance between the untreated and superhydrophobic aluminum alloys, the corrosive products is investigated with XRD analysis. The phase structure of both the untreated and superhydrophobic aluminum alloys corroded for 0 and 90 days was analyzed by XRD technique, and the investigated XRD patterns are shown in Fig. 13. It can be seen from the XRD pattern of the untreated Al alloy plate corroded for 0 days (see Fig. 13a) that four main diffraction peaks present at 2θ of 38.5°, 44.7°, 65.1°, and 78.2°. These crystal peaks are ascribed to the Al phase with orientation planes of (111), (200), (220), and (311), respectively, just as similar to what in JCPDS file No. 85-1327 of the metallic aluminum. Additionally, there are two very low peaks presented at 2θ of 27.1° and 42.6°, which are corresponding to the phase of Al_2O_3 (the JCPDS file No. 73-1199) with orientation planes of (102), (202). Likely, four main diffraction peaks ascribed to the aluminum phase also present at the XRD patterns of both the untreated (Fig. 13b) and superhydrophobic aluminum alloys (Fig. 13c) corroded for 90 days. More importantly, three new sharp and intensive diffraction peaks at 2θ of 18.6°, 20.5°, and 40.7° present in the XRD pattern of the untreated aluminum alloys after corrosion (see Fig. 13b), which are affirmed to be the corresponding crystal planes of $Al(OH)_3$ with orientation planes of (001), (020), (131), just as indexed in the JCPDS file No. 77-0117. By contrast, the intensity of these three diffraction peaks is quite weak so that nearly no corresponding peaks appear for the superhydrophobic Al alloy corroded for 90 days (see Fig. 13c). These results indicate that very litter amount of $Al(OH)_3$ crystals forms on the superhydrophobic surface, which is quite in accordance with the loose nubbly particles appeared on the superhydrophobic surface shown in Fig. 11d.

In summary, it can be inferred that the aforementioned corrosive products deposited on the aluminum alloy surfaces after immersed in NaCl solution are $Al(OH)_3$, and the deposited $Al(OH)_3$ on the superhydrophobic aluminum alloy surfaces is much less than that deposited on the untreated aluminum alloys.

The difference of the microstructure and chemical composition between the untreated and superhydrophobic aluminum alloy surfaces as well as before and after immersion in NaCl solution must be related to the surface morphology, composition, wettability, etc. Moreover, it related to the formation of corrosive products. Such variation is probably because of the following electrochemical reactions [31, 32]:

First, the oxidized layer hydrates in the NaCl solution:

$$Al_2O_3 + 3H_2O \rightarrow 2Al(OH)_3 \quad (3)$$

Then, the resultant $Al(OH)_3$ can be dissolved further by aggressive Cl^-:

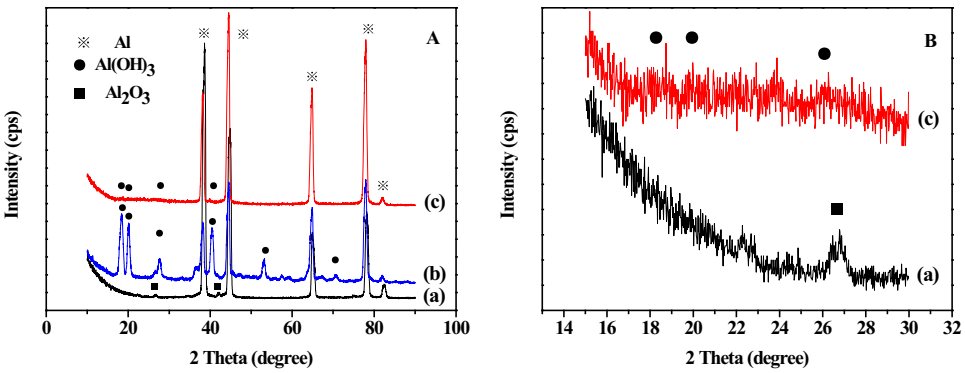

Fig. 13 XRD patterns of the aluminum alloy plates after immersed in 3.5 wt% of NaCl solution for different time: **a** untreated—0 days, **b** untreated—90 days, and **c** superhydrophobic—90 days

$$Al(OH)_3 + Cl^- \rightarrow Al(OH)_2Cl + OH^- \quad (4)$$

$$Al(OH)_2Cl + Cl^- \rightarrow Al(OH)Cl_2 + OH^- \quad (5)$$

$$Al(OH)Cl_2 + Cl^- \rightarrow AlCl_3 + OH^- \quad (6)$$

Meanwhile, the electrochemical reaction of the exposed Al occurs:

$$Al \rightarrow Al^{3+} + 3e^- \quad (7)$$

$$O_2 + H_2O + 4e^- \rightarrow 4OH^- \quad (8)$$

Particularly, once the oxidized layer exposed to NaCl solution, it can reacts with the water and $Al(OH)_3$ is resulted, as shown in Eq. (3). Then, the $Al(OH)_3$ layer would be dissolved by degrees upon the attack of the aggressive Cl^-, [see Eqs. (4)–(6)]. Meanwhile, the exposed Al would be further converted into $Al(OH)_3$ by the electrochemical reactions [see Eqs. (7)–(8)] when the barrier of Al_2O_3 and $Al(OH)_3$ dissolved. The changes of O, Al, and C content in EDS results just show exactly that the corrosion reactions have occurred. Additionally, the Cl and Na elements mentioned above should be the little residual of chloride [can be inferred from Eqs. (4)–(6)] when corroded in NaCl solution. As compared to the untreated aluminum, a strong water-repellent coating exists on the superhydrophobic aluminum alloy surface. Just based on the protection of the strong water-repellent coating, the corrosive ion, such as Cl^-, cannot close and penetrate into the superhydrophobic aluminum alloy surface when the samples are immersed in NaCl solution. As a result, the electrochemical reactions mentioned above will be cut down greatly for the superhydrophobic aluminum alloy than those of the untreated aluminum. Consequently, the corrosive probability is reduced for the superhydrophobic aluminum alloys as compared to the untreated ones. Therefore, the corrosive residual is less for the superhydrophobic aluminum alloy as compared to that of the untreated aluminum alloy.

Both the electrochemical experiments and long-term immersion experiments indicate that the superhydrophobic surface exhibits excellent corrosion resistance. This phenomenon can be well explained by 'Cushion Effect' and 'Capillarity' [3, 27]. Figure 14 shows the interface model for anticorrosion mechanism of the superhydrophobic Al alloy surface in contact with 3.5 wt% of NaCl aqueous solution. The superhydrophobic surface takes on the micro- and nano-dual scales' structure (as shown in Fig. 7) grafted with the long hydrophobic alkyl chains. The hierarchical surface can easily capture great deals of air at the interface, and the long hydrophobic alkyl chains can exclude the hydrophilic media from close. Therefore, an effective barrier obtains so that the water and the corrosive Cl^- cannot enter and contact with the aluminum surface directly, which further hinders the superhydrophobic Al surface from corrosion. However, with the immersion time in 3.5 wt% of NaCl aqueous solution gradually extending, the aggressive Cl^- maybe penetrate into the superhydrophobic surface depends on its priority from the vulnerable and weakest places and the corrosive reaction occurs from now on. So that the wettability of the superhydrophobic Al alloy surface with excellent corrosion resistance decreases, which is consistent with the results of the long-term corrosion resistance experiments, just as affirmed by the equations [Eqs. (3)–(8)] that the exposed Al contacted with 3.5 wt% of NaCl aqueous solution is finally converted to $Al(OH)_3$ through the electrochemical reactions as well. More importantly, the untreated aluminum alloy surface mainly complies with the above corrosive reactions [31], while the corrosion rate is far larger than that of the superhydrophobic ones. This conclusion can also be demonstrated by the corrosion products deposited on the surface from Figs. 9 and 11. Besides, these reactions are responsible for the pitting [33–35] generated on the untreated and superhydrophobic samples. For the superhydrophobic surface, pitting can further peel off the water-repellent film and speeds up the corrosion rate, and this is one of the reasons why the corrosion resistance gradually decreases with the extension of the immersion time in NaCl solution. In conclusion, the superhydrophobic film can greatly improve the corrosion resistance of the aluminum alloy, and the aluminum alloy

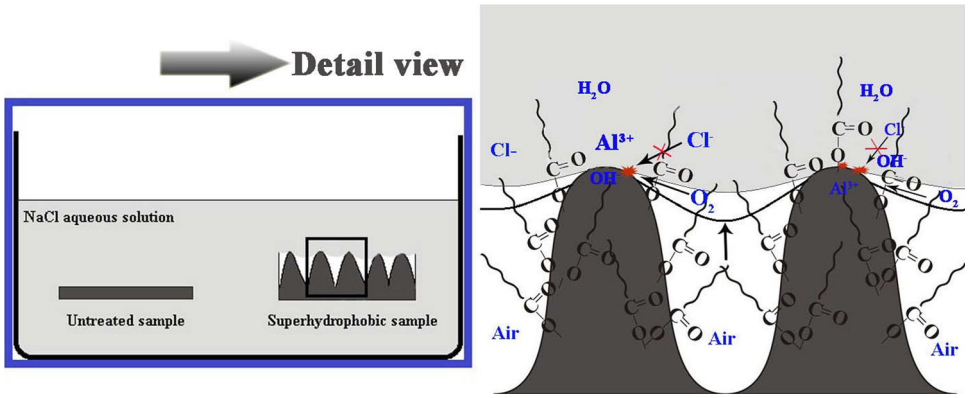

Fig. 14 Interface model for anticorrosion mechanism of the superhydrophobic surface in corrosive NaCl aqueous solution

can be protected effectively in the brine and seawater for limited term.

4 Conclusions

In summary, an effective and facile approach for preparing the superhydrophobic Al alloy surface with excellent corrosion resistance has been proposed. The resultant Al alloy surfaces exhibit a high water contact angle of 156.6° and a low sliding angle of less than 3°. Results show that a porous and rough structure is formed on the Al alloy surface through the boiling water treatment and stearic acid modification. Consequently, the long hydrophobic alkyl chains are chemically grafted onto the rough and porous Al alloy surfaces. The surface wettability of the superhydrophobic samples is greatly influenced by the volume ratio of DMF to water and the STA modification time. The superhydrophobic Al alloy shows excellent corrosion resistance in NaCl solution according to the electrochemical experiments and long-term immersion experiments. What's more, the EDS and XRD tests show that the mainly corrosive products are $Al(OH)_3$, while the $Al(OH)_3$ amount deposited on the superhydrophobic Al alloy surface is quite small than that of the untreated Al alloy. This work puts forward a facile and environment-friendly method for fabricating a flowerlike superhydrophobic Al alloy surface with excellent corrosion resistance, which is favorable for its practical application as an engineering material in seawater corrosion conditions.

Acknowledgements This research is supported by National Natural Science Foundation of China (Grant No. 21161012).

References

1. Z.P. Zuo, R.J. Liao, C. Guo, Y. Yuan, X.T. Zhao, A.Y. Zhuang, Y.Y. Zhang, Fabrication and anti-icing property of coral-like superhydrophobic aluminum surface. Appl. Surf. Sci. **331**, 132–139 (2015)
2. H. Teisala, M. Tuominen, J. Kuusipalo, Superhydrophobic coatings on cellulose-based materials: fabrication, properties, and applications. Adv. Mater. Interfaces **1**, 1300026 (2014)
3. S.L. Zheng, C. Li, Q.T. Fu, M. Li, Q. Wang, Fabrication of self-cleaning superhydrophobic surface on aluminum alloys with excellent corrosion resistance. Surf. Coat. Technol. **276**, 341–348 (2015)
4. G. Song, A. Atrens, D.S. John, X. Wu, J. Nairn, The anodic dissolution of magnesium in chloride and sulphate solutions. Corros. Sci. **39**, 1981–2004 (1997)
5. T. Ishizaki, N. Saito, Rapid formation of a superhydrophobic surface on a magnesium alloy coated with a cerium oxide film by a simple immersion process at room temperature and its chemical stability. Langmuir **26**, 9749–9755 (2010)
6. G.L. Makar, J. Kruger, Corrosion studies of rapidly solidified magnesium alloys. Electrochem. Soc. **137**, 414–421 (1990)
7. G. Song, A. Atrens, D. StJohn, J. Nairn, Y. Li, The electrochemical corrosion of pure magnesium in 1 N NaCl. Corros. Sci. **39**, 855–875 (1997)
8. L.B. Feng, Y.H. Che, Y.H. Liu, X.H. Qiang, Y.P. Wang, Fabrication of superhydrophobic aluminium alloy surface with excellent corrosion resistance by a facile and environment-friendly method. Appl. Surf. Sci. **283**, 367–374 (2013)
9. J. Liang, Y.C. Hu, Y.Q. Wu, H. Chen, Facile formation of superhydrophobic silica-based surface on aluminum substrate with tetraethylorthosilicate and vinyltriethoxysilane as co-precursor and its corrosion resistant performance in corrosive NaCl aqueous solution. Surf. Coat. Technol. **240**, 145–153 (2014)
10. H. Li, S.R. Yu, X.X. Han, Fabrication of CuO hierarchical flower-like structures with biomimetic superamphiphobic, self-cleaning and corrosion resistance properties. Chem. Eng. J. **283**, 1443–1454 (2016)
11. Y. Huang, D.K. Sarkar, X.G. Chen, Superhydrophobic aluminum alloy surfaces prepared by chemical etching process and their corrosion resistance properties. Appl. Surf. Sci. **356**, 1012–1024 (2015)
12. Y.Q. Gao, I. Gereige, A.E. Labban, D. Cha, T.T. Isimjan, P.M. Beaujuge, Highly transparent and UV-resistant superhydrophobic SiO_2− coated ZnO nanorod arrays. ACS Appl. Mater. Interfaces **6**, 2219–2223 (2014)
13. Z. Yu, W. Song, L. Chen, Y. Park, B. Zhao, Q. Cong, Y.M. Jung, Simple immersion to prepare a Zn/Ag biomimetic superhydrophobic surface and exploring its applications on SERS, colloids and surfaces a: physicochem. Eng. Aspects **467**, 224–232 (2015)

14. L.B. Feng, Z.N. Yan, X.H. Qiang, Y.P. Wang, Y.H. Liu, Polystyrene-grafted Al surface with excellent superhydrophobicity and corrosion resistance. Surf. Interface Anal. **47**, 506–513 (2015)
15. Z.W. Wang, Y.L. Su, Q. Li, Y. Liu, Z.X. She, P. Zhang, Researching a highly anti-corrosion superhydrophobic film fabricated on AZ91D magnesium alloy and its anti-bacteria adhesion effect. Mater. Charact. **99**, 200–209 (2015)
16. G. Momen, R. Jafari, M. Farzaneh, Ice repellency behaviour of superhydrophobic surfaces: effects of atmospheric icing conditions and surface roughness. Appl. Surf. Sci. **349**, 211–218 (2015)
17. D.L. Zang, F. Liu, M. Zhang, X.G. Niu, Z.X. Gao, C.Y. Wang, Superhydrophobic coating on fiberglass cloth for selective removal of oil from water. Chem. Eng. J. **262**, 210–216 (2015)
18. Y. Huang, D.K. Sarkar, X.G. Chen, Superhydrophobic nanostructured ZnO thin films on aluminum alloy substrates by electrophoretic deposition process. Appl. Surf. Sci. **327**, 327–334 (2015)
19. S.H. Liu, X.J. Liu, S.S. Latthe, L. Gao, S. An, R.M. Xing, Self-cleaning transparent superhydrophobic coatings through simple sol–gel processing of fluoroalkylsilane. Appl. Surf. Sci. **351**, 897–903 (2015)
20. S.Y. Li, J. Wang, Y. Li, C.W. Wang, Superhydrophobic surface based on self-aggregated alumina nanowire clusters fabricated by anodization. Microelectron. Eng. **142**, 70–76 (2015)
21. R.J. Liao, Z.P. Zuo, C. Guo, Y. Yuan, A.Y. Zhuang, Fabrication of superhydrophobic surface on aluminum by continuous chemical etching and its anti-icing property. Appl. Surf. Sci. **317**, 701–709 (2014)
22. S. Poorebrahimia, R. Norouzbeigi, A facile solution-immersion process for the fabrication of superhydrophobic gibbsite films with a binary micro-nano structure: effective factors optimization via Taguchi method. Appl. Surf. Sci. **356**, 157–166 (2015)
23. L.B. Feng, H.X. Zhang, Z.L. Wang, Y.H. Liu, Superhydrophobic aluminum alloy surface: fabrication, structure, and corrosion resistance. Colloids Surf. A **441**, 319–325 (2014)
24. D.V. Ta, A. Dunn, T.J. Wasley, R.W. Kay, J. Stringer, P.J. Smith, C. Connaughton, J.D. Shephard, Nanosecond laser textured superhydrophobic metallic surfaces and their chemical sensing applications. Appl. Surf. Sci. **357**, 248–254 (2015)
25. A.Y. Vorobyev, C.L. Guo, Multifunctional surfaces produced by femtosecond laser pulses. J. Appl. Phys. **117**, 033103 (2015)
26. X.W. Li, Q.X. Zhang, Z. Guo, T. Shi, J.G. Yu, M.K. Tang, X.J. Huang, Fabrication of superhydrophobic surface with improved corrosion inhibition on 6061 aluminum alloy substrate. Appl. Surf. Sci. **342**, 76–83 (2015)
27. L.B. Feng, L.B. Zhao, X.H. Qiang, Y.H. Liu, Z.Q. Sun, B. Wang, Fabrication of superhydrophobic copper surface with excellent corrosion resistance. Appl. Phys. A **119**, 75–83 (2015)
28. R.N. Wenzel, Surface roughness and contact angle. J. Phys. Org. Chem. **53**, 1466 (1949)
29. M. Ruan, W. Li, B.S. Wang, Optimal conditions for the preparation of superhydrophobic surfaces on al substrates using a simple etching approach. Appl. Surf. Sci. **258**, 7031–7035 (2012)
30. A.B.D. Cassie, S. Baxter, Wettability of porous surfaces. Trans. Faraday Soc. **40**, 546–551 (1944)
31. D.M. Lv, J.F. Ou, M.S. Xue, F.J. Wang, Stability and corrosion resistance of superhydrophobic surface on oxidized aluminum in NaCl aqueous solution. Appl. Surf. Sci. **333**, 163–169 (2015)
32. S.M. Moon, S.I. Ryun, Faradaic reactions and their effects on dissolution of the natural oxide film on pure aluminum during cathodic polarization in aqueous solutions. Corros. Sci. **54**, 546 (1998)
33. W.H. Alior, Evaluation of aluminum after one-year deep sea exposure. J. Hydronaut. **2**, 26–33 (1968)
34. C.M. Liao, J.M. Olive, M. Gao, In-situ monitoring of pitting corrosion in aluminum alloy 2024. Corrosion **54**, 451–458 (1998)
35. C.M. Liao, R.P. Wei, Galvanic coupling of model alloys to aluminum: a foundation for understanding particle-induced pitting in aluminum alloys. Electrochimica Acta. **45**, 881–888 (1999)